

## Journal Pre-proofs

Optimisation of metastable supercooled liquid phase change material for long-term heat energy accumulation

Jiří Ryšavý, Jakub Čespiva, Thangavel Sangeetha, Christian Teicht, Matěj Charvát, Wei-Mon Yan, Ricardo Chacartegui, Tadeáš Ochodek

PII: S2590-1745(25)00193-X  
DOI: <https://doi.org/10.1016/j.ecmx.2025.101061>  
Reference: ECMX 101061

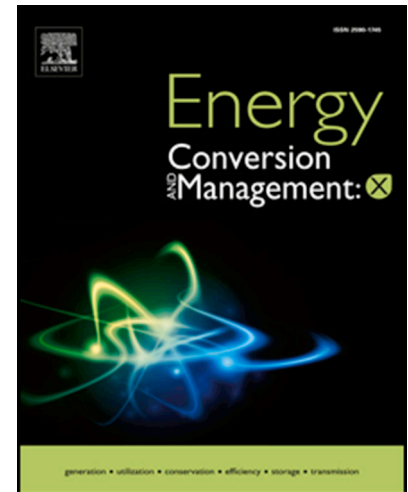
To appear in: *Energy Conversion and Management: X*

Received Date: 22 December 2024  
Revised Date: 5 April 2025  
Accepted Date: 10 May 2025

Please cite this article as: J. Ryšavý, J. Čespiva, T. Sangeetha, C. Teicht, M. Charvát, W-M. Yan, R. Chacartegui, T. Ochodek, Optimisation of metastable supercooled liquid phase change material for long-term heat energy accumulation, *Energy Conversion and Management: X* (2025), doi: <https://doi.org/10.1016/j.ecmx.2025.101061>

This is a PDF file of an article that has undergone enhancements after acceptance, such as the addition of a cover page and metadata, and formatting for readability, but it is not yet the definitive version of record. This version will undergo additional copyediting, typesetting and review before it is published in its final form, but we are providing this version to give early visibility of the article. Please note that, during the production process, errors may be discovered which could affect the content, and all legal disclaimers that apply to the journal pertain.

© 2025 Published by Elsevier Ltd.



Authors:

Jiří Ryšavý\*<sup>1</sup> – [jiri.rysavý@vsb.cz](mailto:jiri.rysavý@vsb.cz) – corresponding author

Jakub Čespiva<sup>1</sup> – [jakub.cespiva@vsb.cz](mailto:jakub.cespiva@vsb.cz)

Thangavel Sangeetha<sup>2</sup> - [sangeetha@mail.ntut.edu.tw](mailto:sangeetha@mail.ntut.edu.tw)

Christian Teicht<sup>3</sup> - [christian.teicht@ict.fraunhofer.de](mailto:christian.teicht@ict.fraunhofer.de)

Matěj Charvát<sup>1</sup> – [matej.charvat@vsb.cz](mailto:matej.charvat@vsb.cz)

Wei-Mon Yan<sup>2,4</sup> - [wmyan@ntut.edu.tw](mailto:wmyan@ntut.edu.tw)

Ricardo Chacartegui<sup>5,6</sup> - [ricardoch@us.es](mailto:ricardoch@us.es)

Tadeáš Ochodek<sup>1</sup> – [tadeas.ochodek@vsb.cz](mailto:tadeas.ochodek@vsb.cz)

<sup>1</sup>Energy Research Centre, Centre for Energy and Environmental Technologies, VSB – Technical University of Ostrava, 17. listopadu 2172/15, Ostrava-Poruba, 70800, Czech Republic

<sup>2</sup>Department of Energy and Refrigerating Air-Conditioning Engineering, National Taipei University of Technology, Taipei 10608, Taiwan

<sup>3</sup>Fraunhofer Institute for Chemical Technology (ICT), Joseph-von-Fraunhofer Str. 7, 76327, Pfinztal, Germany

<sup>4</sup>Research Center of Energy Conservation for New Generation of Residential, Commercial, and Industrial Sectors, National Taipei University of Technology, Taipei 10608, Taiwan

<sup>5</sup>University of Seville, Escuela Técnica Superior de Ingenieros, Camino de los Descubrimientos s/n, 41092 Seville, Spain

<sup>6</sup>University of Seville, Laboratory of Engineering for Energy and Environmental Sustainability, Seville 41092, Spain

## ABSTRACT

This research study investigates sodium acetate trihydrate as a metastable supercooled liquid phase change material for long-term heat energy storage and is an efficient evaluation of various sodium acetate trihydrate-to-water ratios and heat exchanger geometries to enhance storage efficiency. Experimental modules with spiral and toroid squiggle heat exchangers were developed to assess energy retention during liquefaction, sensible heat discharge, and latent heat discharge phases. Experimental outcomes indicate that the toroid squiggle design extends latent heat discharge duration by up to 35 minutes compared to the spiral exchanger, reaching a maximum of 29 minutes. The optimal sodium acetate trihydrate-to-water ratio was 92%, balancing high theoretical latent heat capacity (93.6 Wh) and low theoretical to real latent heat capacity ratio with phase stability. The toroid squiggle exchanger with the mentioned accumulation substance demonstrated better heat transfer, maintaining energy output above 100 W for 11 minutes and above 50 W for 35 minutes, while the spiral design showed lower values, retaining above 100 W for only 7 minutes and above 50 W for 26 minutes. Furthermore, specific heat capacity measurements showed that sodium acetate trihydrate-to-water 92:8 ratio (SAT 92) exhibited specific heat values of 2.1 kJ/kg·K in the solid phase and 5.0 kJ/kg·K in the liquid phase, confirming its strong thermal storage potential with minimal phase instability. The conclusions have highlighted the importance of optimizing heat exchanger geometry and sodium acetate trihydrate composition for sustainable energy storage and these

40 significant insights will contribute to improving seasonal heat accumulation technologies, particularly in synergy with  
41 rene

42  
43 **KEYWORDS**

44 Supercooled liquid storage; PCM phase stability; Latent heat discharge; Heat exchanger optimization; Thermal energy  
45 retention

46  
47 **ABBREVIATIONS**

48	COP	Coefficient of Performance
49	$c_p$	Specific heat capacity of each material forming the accumulation module and accumulation substance 50 (calculated as a function reflecting the temperature change according to the formula presented by 51 Beaupere et al. [12]) [ $J \cdot kg^{-1} \cdot K^{-1}$ ]
52	DL	Data Logger
53	DSC	Differential Scanning Calorimetry
54	H <sub>2</sub> O	Water
55	H <sub>x</sub>	Heat Exchanger
56	L	Specific theoretical latent heat of solidification [ $kJ \cdot kg^{-1}$ ]
57	m	Weight of each material forming the accumulation module; weight of accumulation substance [kg]
58	$\dot{m}$	Mass Flow Rate [ $kg \cdot s^{-1}$ ]
59	MSLPCM	Metastable Supercooled Liquid Phase Change Material
60	P	Heat Power [W]
61	PCM	Phase Change Material
62	PE	Polyethylene
63	Q	Heat Energy [J, Wh]
64	$Q_{char\_diff}$	The difference between $Q_{char\_teor}$ and $Q_{char\_real}$ [%]
65	$Q_{char\_real}$	The real charge heat required to heat up the entire module and liquefy the accumulation substance [J, 66 Wh]
67	$Q_{char\_teor}$	The theoretical charge heat required to heat the entire module and liquefy the accumulation substance 68 (equivalent to $Q_{dischar\_teor}$ ) [J, Wh]
69	$Q_{L\_teor}$	Theoretical latent heat of solidification [J, Wh]
70	$Q_{L\_diff}$	The difference between $Q_{char\_teor}$ and $Q_{char\_real}$ [%]
71	$Q_{L\_real}$	The real discharge heat energy emitted from the entire module during discharge of latent heat phase [J, 72 Wh]
73	$Q_{sen\_teor}$	The theoretical discharge heat energy required to heat the entire [J, Wh]

74	$Q_{\text{sen\_real}}$	The real discharge heat energy emitted from the entire module during discharge of sensible heat phase
75		
76	$Q_{\text{sen\_diff}}$	The difference between $Q_{\text{char\_teor}}$ and $Q_{\text{char\_real}}$ [%]
77	SAT	Sodium Acetate Trihydrate
78	$T_o$	Onset Temperature (solid phase initiation) [°C]
79	$T_f$	Final Temperature (end of phase transition) [°C]
80	$T_i$	Onset of Liquid Phase [°C]
81	$T_{\text{max}}$	Peak Temperature (maximum phase change activity) [°C]
82	$\Delta T$	Temperature Difference [K]
83	$\omega_{\text{SA}}$	Mass fraction of sodium acetate in the accumulation substance [%]
84		

## 85 INTRODUCTION

86 Long-term or seasonal heat energy accumulation is becoming an increasingly prominent topic on various platforms,  
 87 from energy experts to politics. Water accumulation in tanks has several advantages and is a widely employed technique.  
 88 However, it implies only sensible heat, and from the long-term thermal energy storage perspective, it implies high  
 89 insulation requirements, penalising sizing and costs [1].

90 The long-term storage of heat energy between seasons can significantly reduce the mismatch between heat supply and  
 91 demand, which is particularly suitable in synergy with renewable energy sources [2] or, for example, heat pumps, whose  
 92 COP varies significantly between seasons and can also use renewable energy [3]. These systems can also significantly  
 93 increase the self-consumption of households or communities, which is crucial in terms of the profitability of renewable  
 94 energy sources [4].

95 Phase change materials (PCM) store thermal energy as sensible and latent heat, which can reduce the required storage  
 96 volume for a given thermal energy capacity [5]. These materials are gradually being employed not only in the energy  
 97 industry sector, for example, as thermal compensators for electronics [6] or as an efficiency enhancer for solar  
 98 desalination systems [7, 8], but also in the household sector, where they are implemented with advantages, for example,  
 99 in supposed Zero-Energy Buildings [9], as a part of concentrated photovoltaic and thermal systems [10] or as latent heat  
 100 storage systems utilised for solar cookers [11]. In the case of incorporating PCM into building energy systems, the  
 101 efficiency of renewable energy utilisation and thermal comfort can be improved [12]; therefore, energy costs and carbon  
 102 footprint can be reduced [13]. Although conventional PCM materials can significantly increase the rate of heat storage,  
 103 their use for long-term heat storage for long-term periods (months) is very limited [14].

104 Metastable supercooled liquid phase change materials (MSLPCM) are characterised by enduring in the liquid state even  
 105 at temperatures below the melting point [15]. Unlike standard PCMs (paraffins, olefins, etc.), their solidification process  
 106 can be purposefully initiated with a consequent latent heat release. This phenomenon offers a wide range of possibilities  
 107 for combined long and short-term energy storage [16]. MSLPCMs differ predominantly in characteristics like melting  
 108 temperature, latent heat of solidification, and specific heat capacity (in liquid and solid phases). The sodium acetate  
 109 trihydrate (SAT) is one of the most promising MSLPCMs for household heating and hot water conditioning thermal  
 110 energy storage applications [17]. The theoretical SAT latent heat of solidification is 264 kJ/kg at the melting point of  
 111 58 °C [18]. Specific heat capacity in solid and liquid phase is  $c_{p(s)} = 2.03 \text{ kJ}\cdot\text{kg}^{-1}\cdot\text{K}^{-1}$  and  $c_{p(l)} = 3.01 \text{ kJ}\cdot\text{kg}^{-1}\cdot\text{K}^{-1}$  [19].

112 Despite the promising properties of SAT (high energy storage density, large supercooling degree, high latent heat, non-  
 113 toxicity, low cost), there are some drawbacks, such as low heat exchange capacity rate, phase separation, spontaneous  
 114 crystallisation, low thermal conductivity effect, unstable supercooling or corrosion with commonly used metals [16].  
 115 Several issues, such as the scaling effect, storage time, triggering of solidification and heat delivery control, still require  
 116 in-depth understanding and solving before implementing SAT as an accumulation medium in industries. The most  
 117 significant one among them is spontaneous partial crystallisation, which induces a reduction of the utilisable energy,  
 118 and is especially crucial in seasonal heat energy storage applications. One of the most considered solutions to prevent  
 119 this undesired crystallisation is to enrich SAT with additives such as water, the most common and affordable option

120 [20]. Research indicates that adding water to SAT improves phase stability and reduces problems like incongruent  
121 mel; the  
122 effective amount of the phase-change material per unit mass decreases [21].

123 Previous research studies have investigated SAT with additional water contents: Dannemand et al. [22] (9 %<sub>wt.</sub>),  
124 Dannemand et al. [23] (6.4 %<sub>wt.</sub>), Englmaier [24] (2 %<sub>wt.</sub>), and Kafle et al. [25] (5.1 and 9.2%<sub>wt.</sub>). On the other hand,  
125 several studies, such as Nohejl [26] and Dannemand et al. [22, 27] presented results of experiments with SAT without  
126 extra-added water (above the trihydrate level). They have reported and proved the presumption of the low success rate  
127 of controlling the supercooled liquid phase even after proper liquefaction, which means that the process of crystallisation  
128 was triggered spontaneously with a higher probability than in the case of extra water added. Maintenance of the liquid  
129 phase is critical for successful long-term heat accumulation [28]. The water-to-SAT weight ratio is crucial for attaining  
130 the highest energy storage density, and this is a yet unsolved research bottleneck, and its significant impact on the  
131 different challenges for the successful implementation of SAT for thermal energy storage in buildings [20]. It is essential  
132 to adapt the protocol for a properly selected accumulation mixture to the way of its use from alone standing or, e.g.  
133 brick-integrated capsules containing PCM (SAT) [29], through purposefully designed and constructed heat exchangers  
134 with internal PCM volume [30], to the innovative approaches such as introducing jet breakup of PCM [31].

135 This research is an attempt to address a significant literature gap concerning optimising metastable supercooled liquid  
136 PCM for prolonged thermal energy storage. Although earlier research studies have explored sodium acetate trihydrate  
137 as a PCM, there is a notable absence of investigations that systematically integrate heat exchanger geometry with  
138 optimised sodium acetate-to-water ratios to enhance sensible and latent heat discharge performance. The novelty of this  
139 present study is that it highlights the unique combination of experimental and theoretical approaches to evaluate the  
140 synergy between PCM composition and heat exchanger design, leading to improved energy retention and phase stability.

141 To systematically investigate these factors, a dedicated test bench was constructed to assess the charging and discharging  
142 performance of latent heat storage systems. The setup includes a testing rig designed to measure energy flows and heat  
143 accumulation in PCM-filled heat exchanger modules with controlled experimental conditions.

144 Our investigation also introduces and compares two heat exchanger designs, such as spiral and toroid squiggle, to  
145 identify the configuration that maximises energy retention while minimising phase instability.

146 Integration of experimental measurements with theoretical calculations will bridge the gap between the predicted and  
147 observed thermal behaviours, thereby establishing a novel framework for long-term heat energy accumulation.

## 148 MATERIALS AND METHODS

149 This section describes the preparation of the SAT mixtures, the manufacture of the PCM-filled heat exchanger modules,  
150 and the test apparatus constructed and used.

### 151 Accumulation substance

152 The SAT required for this study was purchased in a food grade from a company called FICHEMA Ltd. (Czech  
153 Republic). Physico-chemical parameters of the sample provided by the producer are listed in Table 1. The water added  
154 was demineralised to high purity with conductivity less than 0.1  $\mu\text{S}\cdot\text{cm}^{-1}$ .

156 *Table 1 Physical chemical parameters of used SAT [32]*

Physical chemical parameters of used SAT	
SAT content	min. 99 % <sub>wt.</sub>
Weight loss by drying	36 - 41 % <sub>wt.</sub>
pH (1 %)	8.0 - 9.5

As max. 3 ppm

Pb max. 2 ppm

Hg max. 1 ppm

Oxidizable subst. max. 1000 mg·kg<sup>-1</sup> (as HCOOH)

157

158 The SAT or SAT/H<sub>2</sub>O substance was loaded in resealable laboratory glass bottles (2,000 ml) and heated in the oven at  
 159 90 °C for 24 hours to ensure complete substance melting. Later on, the accumulation module was filled with the liquified  
 160 SAT/H<sub>2</sub>O substance and enclosed while the final weight of the whole SAT/H<sub>2</sub>O substance was equal to 1,750 g every  
 161 time. Once the measurement was completed, the accumulation substance was heated at 90 °C, retrieved from the module  
 162 in the liquid, and replaced with samples with different SAT/H<sub>2</sub>O ratios at a warm state.

163 Various SAT/H<sub>2</sub>O ratios were examined and compared from the functionality, energy storage and reliability points of  
 164 view. The SAT was blended in different proportions with water (4, 6, 8 and 10 %<sub>w.t.</sub>) while maintaining the final weight  
 165 of the SAT/H<sub>2</sub>O sample. Table 2 represents the ratios between anhydrite sodium acetate and water in the mixtures used  
 166 for SAT 96 and SAT 90. The accumulation substances consisted of SAT and additional water, which were marked for  
 167 the purpose of this study according to the mass fraction of SAT in the substance, while the rest of the substance was  
 168 additional water.

169

170

171

*Table 2 Physical chemical parameters of used SAT*

	Sodium acetate (anhydrite)	Water
	[%]	[%]
SAT 96	57.9	42.1
SAT 94	56.7	43.3
SAT 92	55.5	44.5
SAT 90	54.3	45.7

172

173

### Measurement of specific heat capacity $c_p$

174 The specific heat capacity of SAT 90 and SAT 92 was measured using the highly sensitive differential scanning  
 175 calorimeter (DSC) (PerkinElmer Diamond, USA). This device was operated with two furnaces, enabling precise

176 temperature control with heating and cooling rates of up to 500 °C/min. For this study, the samples of SAT 90 and SAT  
177 92 v Journal Pre-proofs ring  
178 uniform temperature increment throughout the sample.

179 Understanding specific heat capacity is very essential for this research study, as it quantifies the energy required to raise  
180 the temperature of the substance, which is a vital parameter in optimizing the thermal storage properties of PCMs.

### 182 Tested PCM heat exchangers

183 For this study, a testing rig for the determination of energy flows and heat energy accumulation abilities was developed  
184 to compare the performance of different SAT/H<sub>2</sub>O substances within tailored test modules. Two geometrically different  
185 shapes of heat exchangers were constructed: 1) spiral and 2) toroid squiggle (Fig. 1).



187  
188 *Fig. 1. Test module heat exchangers: A Spiral, B Toroid squiggle.*

189 The test module (M) was made of 3 mm thick glass with an inner diameter of 135 mm and with a screw lid in the upper  
190 part equipped with sealing rubber. In this module, each SAT/H<sub>2</sub>O substance was tested while all three separate phases,  
191 including charge (liquefaction), discharge of sensible heat (liquid cooling) and discharge of latent heat (solid cooling  
192 after initiation), were measured and examined. The solidification process was initiated by injecting a tiny SAT crystal  
193 seed into the accumulation substance through one of the tight, closable openings in the lid.

194 The selection of spiral and toroid squiggle heat exchanger geometries was based on pre-experiments as well as on their  
195 potential to enhance heat transfer efficiency while accommodating the specific thermal and phase transition  
196 characteristics of SAT. Previous research studies by Oudaoui et al. [33], and Sultan et al. [34]) have highlighted the  
197 critical role of heat exchanger geometry, particularly during phase changes. The spiral heat exchanger was chosen for  
198 its ability to provide uniform heat distribution from the bottom of the accumulation module in an upward manner, while  
199 leveraging the thermal stratification of liquids, which could optimistically influence the phase transition. Moreover,  
200 spiral heat exchangers have been commonly used in water-based thermal storage systems, as in commercial  
201 accumulation vessels (e.g., Dražice NAD v4).

202 The toroid squiggle geometry was introduced as an alternative to enhance convective heat transfer while minimising  
203 loca Journal Pre-proofs it of  
204 the accumulation module. Additional advantage of the toroid squiggle heat exchanger is its reduced distance between  
205 heat exchanger surfaces or between the heat exchanger and the accumulation module walls, accelerating heat transfer  
206 and extending the higher heat energy output period.

207 By comparing these two designs with similar surface areas, this study is focussed on the evaluation of the impacts of  
208 flow dynamics on heat transfer efficiency and phase stability.

209 The heat exchanger was made from a copper tube with an outer diameter of 8 mm and a wall thickness of 0.5 mm. In  
210 both scenarios, the overall heat exchange surface (outer surface of the heat exchanger) was equal to approximately  
211 33,000 mm<sup>2</sup>.

### 213 Testing rig

214 The testing rig consisted of a cold-collection vessel (V1), into which the water from the building water supply was filled  
215 as required periodically during the measurement to preserve a constant water level. This sufficed with the uniform  
216 (laboratory) temperature and flow of this heat transfer medium. In order to transport the heat transfer medium into the  
217 downstream segments, a universal circulator pump (P) Universal 600 (Eheim, Germany) was used. The circulator pump  
218 was equipped with an inner pre-filter, and its nominal performance was 600 l·h<sup>-1</sup>. An inductive digital flowmeter MIM-  
219 1201H G2 C3T0 (KOBOLD Messring GmbH; Germany) with a manual flow regulation valve (F) was placed behind  
220 the pump. The mass flow of the heat transfer medium was retained at 100±10 g·min<sup>-1</sup> in the case of all measurements  
221 and during all charge and discharge phases of the test module. The slight differences in the mass flow were caused by  
222 changes in the water level in the cold-collection vessel and by variations in the temperature of the pipes within the  
223 experiment.

224 The purpose of the heat exchanger (Hx) was to provide heat to the heat transfer medium during the liquefaction phase  
225 of the SAT/H<sub>2</sub>O substance in the module, and it was placed in front of the test module. The regulated flow heater utilised  
226 electricity via resistance wire for heat generation. During the discharging phase of the test module, the heat source was  
227 turned off, and the inner temperature was equal to that of the whole water system due to the low accumulation capacity  
228 of the heater.

229 The whole test module was placed in a 50 mm thick poly-ethylene insulation shell (PE) to avoid excessive heat losses  
230 to the surroundings during the experiments. Four thermocouples were mounted on the test module: (T1) and (T2) (both  
231 K type) at the heat transfer medium input and output, respectively, and (T3) and (T4) (both T type) at the outer surface  
232 of the test module. The thermocouples were attached to the data logger (DL) SDL200 (Extech Instruments, USA) with  
233 60s-period data logging. The spent heat transfer medium was disposed into a heat-collection vessel (V2) and disposed  
234 off at need. The scheme of the whole testing device for energy flow and accumulation determination has been exhibited  
235 in Fig. 2. The detailed description of measuring methods including measuring range and accuracy is presented in Table  
236 3.

237  
238 *Table 3 Description of measuring methods including measuring range and accuracy*

Device and measured component	Range	Principle	Accuracy
<i>Flow meter MIM-1201H G2 C3T0</i>			
Volume flow	0.01 - 1 l/min	Magnetic-inductive measuring	± (0.8% of reading + 0.5% of FS)
<i>Thermocouple, Type K, class 1</i>			
Cooling, heating temperature	- 50 to 1000 °C	Thermoelectric effect	± 0.3 °C of the measured value

Surface temperature                      - 50 to 250 °                      Thermoelectric effect                       $\pm 0.2$  °C of the measured value

Scale XS Balance BL30

Weight    0 – 30,000 g                      Strain gauge load cell                       $\pm 0.2$  g

Note: The accuracies of the thermocouples were based on their calibration protocol. The uncertainty of the SDL200 datalogger was not taken into consideration. According to GUM (guide of uncertainty in measurement), we have correlated offset errors due to the cold junction compensation that crosses out for the temperature difference. The accuracy of the temperature difference is better than the uncertainty of the absolute measured temperature value.

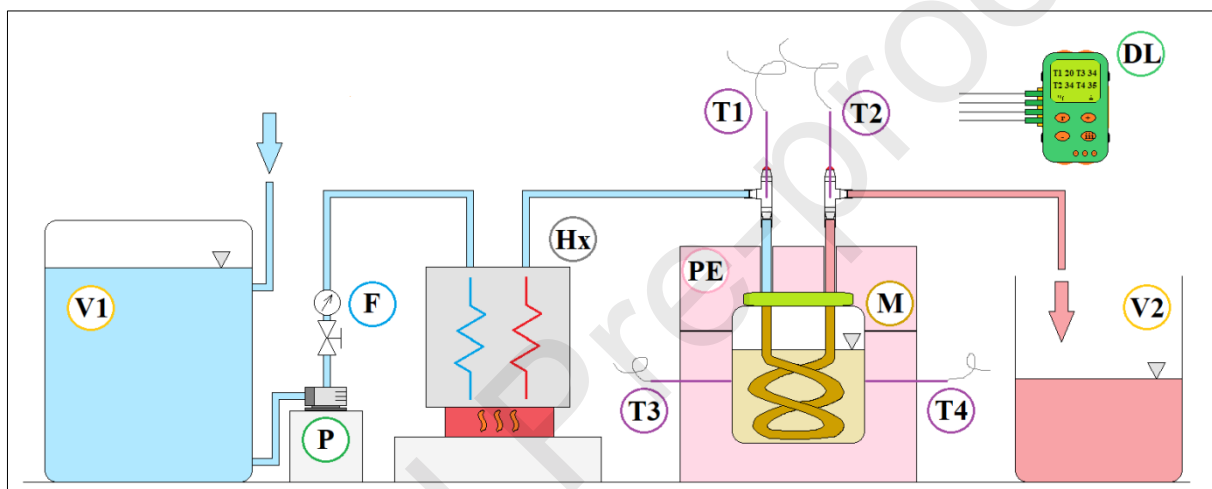


Fig. 2. Energy flow and accumulation testing device scheme. (discharge of latent heat)

## Measurement procedure

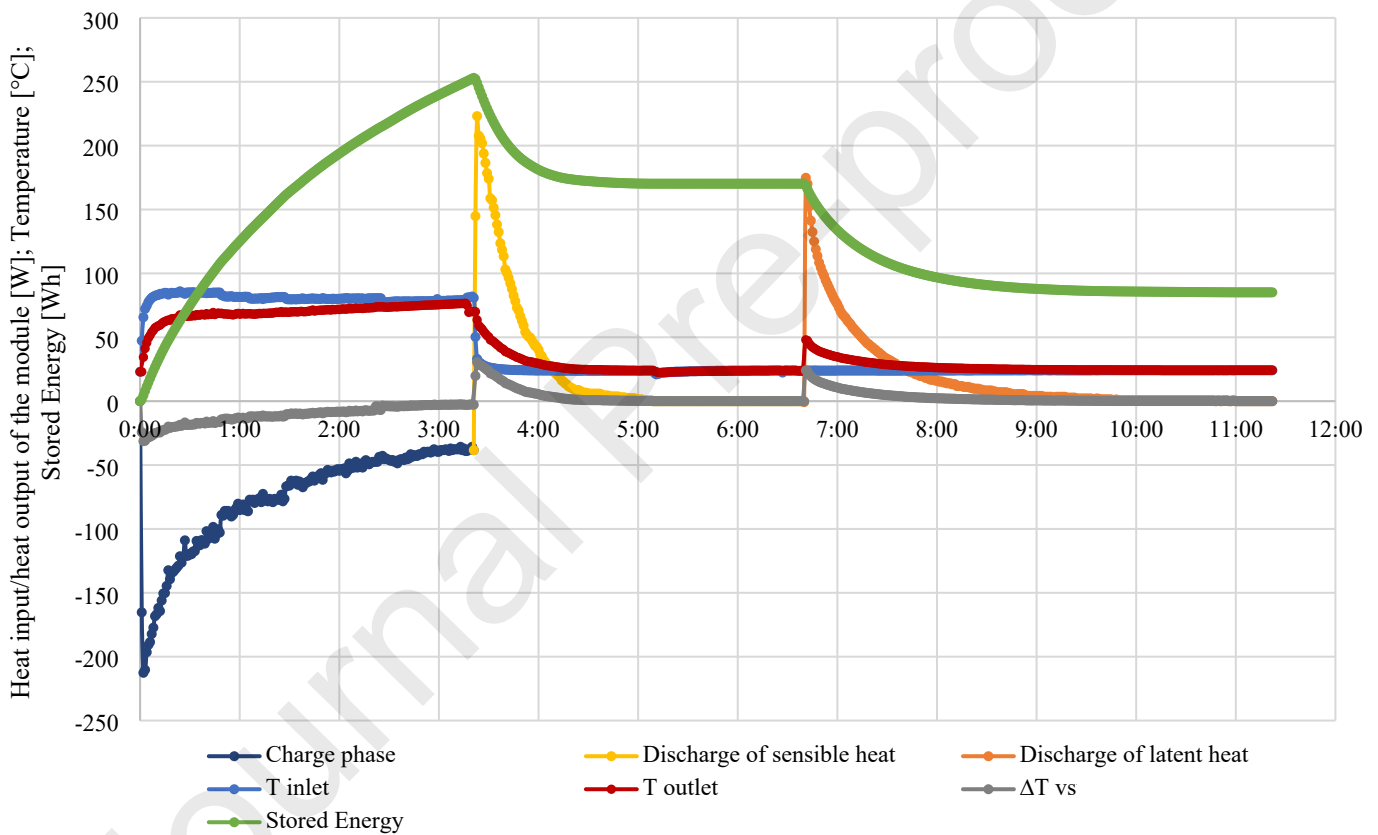
The measurement process commenced by establishing a stable mass flow of water through the entire system without applying any heating. The cold-collection vessel was continuously refilled using the water supply system to maintain a consistent water level, which could influence the mass flow. Before entering the collection vessel, the water from the supply was pre-heated by ambient air in the laboratory via a pre-vessel. The laboratory temperature ranged between 20 and 24 °C and was maintained constant during each individual experiment.

The heating phase was started once all four monitored temperatures (T1–T4) were stabilised to the ambient laboratory temperature. This phase was terminated when the entire volume of the accumulation material transitioned to a liquid state. The state of the accumulation material was visually inspected at regular intervals after the average temperature on the outer surface of the module exceeded 75 °C. Following the heating phase, the discharge of sensible heat commenced and continued until all measured temperatures returned to the ambient laboratory level. Afterwards, the accumulation material was initiated, and the discharge of the sensible heat phase continued until all measured temperatures returned to the ambient laboratory level.

The stabilisation phase, during which all four monitored temperatures (T1–T4) equilibrated to the ambient laboratory temperature—before heating, after the discharge of sensible heat, and after the discharge of latent heat—served as a three-stage justification check for the thermocouples in each measurement cycle. This systematic approach significantly reduced measurement errors and uncertainties. Additionally, the thermocouples were calibrated by calibration institute (Meros, spol. s.r.o.; Czech Republic) and inhouse validated both prior and after the measurement campaign using a JOFRA ATC 650 B temperature calibrator, further ensuring the accuracy and reliability of the recorded data. The equilibrium states were maintained for approximately one hour before initiating the discharge of latent heat. The

268  
 269 **Results evaluation**

270  
 271 Fig. 3 has illustrated the thermal behaviour of the entire accumulation module during all three phases: the charging  
 272 phase, the discharge of sensible heat, and the discharge of latent heat, as obtained from the previously described  
 273 measurement setup. The discharges of sensible and latent heat were analysed in detail for all measured configurations  
 274 in the Results and Discussion section. The stored energy curve represented the time-enthalpy relationship, showing the  
 275 energy stored and released during these periods. The endpoint of this curve reflected the overall process efficiency,  
 276 accounting for heat losses that must be compensated for in a single cycle.



278  
 279 *Fig. 3. Example of the energy flow into and out of the accumulation module during a selected experiment with the SAT 96 accumulation*  
 280 *substance for the Toroid squiggle accumulation module*

281 The actual heat energy input and outputs were calculated for each minute interval during the measurement period  
 282 according to Equation 1, following the basic heat equation originating from the first law of thermodynamics. The  
 283 variable  $P$  represents the heat energy input or output, expressed in watts [W]. The term  $\dot{m}$  denotes the mass flow rate of  
 284 the cooling or heating water, measured in kilograms per second [ $\text{kg}\cdot\text{s}^{-1}$ ]. The parameter  $c_p$  corresponds to the specific  
 285 heat capacity of the cooling or heating water, given in joules per kilogram per kelvin [ $\text{J}\cdot\text{kg}^{-1}\cdot\text{K}^{-1}$ ]. Finally,  $\Delta T$  signifies  
 286 the temperature difference of the cooling and heating water, measured in kelvins [K].

287  
 288 
$$P = \dot{m} \cdot c_p \cdot \Delta T$$

(1)

289

290 The heat energy input and output values were recalculated into the transferred heat energy, denoted as  $O$  in joules [J],  
291 for (Journal Pre-proofs) the  
292 module was determined by integration of Equation (1) over time represented as Equation 2.

$$294 \quad E = \int P dt = \int \dot{m} \cdot c_p \cdot \Delta T dt \quad (2)$$

295  
296 The total amount of heat energy either supplied to or extracted from the module was determined by summing up the  
297 transferred heat values over all minute intervals within the observed phase. This process has been vividly represented in  
298 Fig. 3, where the area between the charge phase curve and the x-axis corresponded to the energy supplied to the  
299 accumulation module. Conversely, the areas beneath both discharge curves and the x-axis illustrated the energy extracted  
300 from the module during the discharge phases. The actual heat energy input and output for all phases were also  
301 theoretically determined to enable further comparison. The theoretical heat energy required for the charge phase was  
302 calculated using the following equations. The total theoretical charge heat energy, represented as  $Q_{char\_teor}$ , consists of  
303 the sum of the theoretical sensible heat,  $Q_{sen\_teor}$ , and the theoretical latent heat of solidification,  $Q_{L\_teor}$ , as expressed  
304 in Equation (3). The theoretical charge heat energy can be further expanded using Equation (4), which accounts for the  
305 sum of the product of the mass of each material forming the accumulation module,  $m$  [kg], its specific heat capacity,  $c_p$   
306 [ $J \cdot kg^{-1} \cdot K^{-1}$ ], and the temperature difference,  $\Delta T$  [K], along with the contribution of the latent heat of solidification,  $L$   
307 multiplied by the material mass. Additionally, the theoretical latent heat of solidification has been determined by  
308 Equation (5), incorporating the mass fraction of sodium acetate in the accumulation substance,  $\omega_{SA}$  in [%] according to  
309 Beuparte et al. [20].

$$311 \quad Q_{char\_teor} = Q_{sen\_teor} + Q_{L\_teor} \quad (3)$$

$$312 \quad Q_{char\_teor} = \sum m \cdot c_p \cdot \Delta T + L \cdot m \quad (4)$$

$$313 \quad Q_{L\_char\_teor} = -462 + 11.8\omega_{SA} \quad (5)$$

314  
315 The achieved temperature differences for the theoretical calculation corresponded to the temperature differences in  
316 actual tests. Theoretical heat energy for discharge of the sensible heat phase and the latent heat phase were calculated  
317 analogically with only one part of Equation 3.

## 318 RESULTS AND DISCUSSION

319 The duration of the charge period consistently was within a limited time range (2:50 and 3:27 [hh:mm]), while the  
320 discharge of sensible heat and latent heat phases also varied within specific time intervals (1:48–3:18 [hh:mm] and 3:31–  
321 7:41 [hh:mm] respectively). The exact timings were dependent on factors such as the shape of the heat exchanger and  
322 the composition of the accumulation substance (particularly the water mass concentration), which influenced the heat  
323 flux, especially during the solidification process. The duration of the whole individual period has been tabulated in Table  
324 4.

325 The end of the discharging phases was determined when the temperature difference in the cooling medium (inlet and  
326 outlet) stabilised to less than 0.1 °C. However, near the end of both discharging phases, prolonged periods were often  
327 characterised by temperature differences as low as 0.1 °C, which could have significantly affected the overall phase  
328 durations.

329 For a more objective comparison of cooling rates, the analysis focused on the time intervals when the heat energy output  
330 exceeded specific thresholds: 150 W during the sensible heat discharge phase and 100 W or 50 W during both phases  
331 (discharge sensible and latent heat) was performed, while the results are presented in Table 4. Table 4 has provided a  
332 detailed comparison of the thermal performance of both heat exchanger designs with varying compositions of the  
333 accumulation substance (SAT concentration). The heat energy output profiles for the discharge of sensible heat and the  
334 discharge of latent heat are illustrated in Figure 4 and Figure 5.

Heat exchanger	Accumulation substance	Heating		Discharge of sensible heat			Discharge of latent heat			Maximal reached temperature (Average T3 and T4)
		Whole period duration	Whole period duration	Heat energy output above 150 W	Heat energy output above 100 W	Heat energy output above 50 W	Whole period duration	Heat energy output above 100 W	Heat energy output above 50 W	
[-]	[%]			[hh:mm]	[hh:mm]	[hh:mm]		[hh:mm]	[hh:mm]	[°C]
Spiral	SAT 94	2:50	2:16	0:13	0:20	0:31	4:50	0:08	0:29	57.0 ± 0.4
Spiral	SAT 92	3:14	2:46	0:13	0:20	0:32	7:41	0:07	0:26	56.1 ± 0.4
Spiral	SAT 90	2:54	2:06	0:13	0:20	0:32	4:16	0:05	0:23	54.6 ± 0.4
Toroid squiggle	SAT 96	3:21	1:48	0:12	0:20	0:33	4:42	0:11	0:32	55.8 ± 0.4
Toroid squiggle	SAT 94	2:56	3:02	0:13	0:20	0:34	3:31	0:11	0:32	54.3 ± 0.4
Toroid squiggle	SAT 92	3:27	3:18	0:12	0:20	0:35	3:47	0:11	0:35	55.6 ± 0.4
Toroid squiggle	SAT 90	2:57	2:30	0:12	0:19	0:32	3:49	0:09	0:32	54.5 ± 0.4

337

338 From the presented data, it is evident that there is no significant difference between both heat exchanger constructions  
339 during the discharge of sensible heat period, whereby the periods of maintaining the heat energy output above 150 W,  
340 100 W, and 50 W did not significantly differ. In the case of the cooling of the liquid substance, significant free  
341 convection occurred in the module, which expunged the differences between the heat exchanger designs (shaping), and  
342 it only favoured the total surface area of the heat exchanger, which was similar in both cases, proving that the results  
343 were almost identical. The study of Garoosi et al. [35] discussed the effects of free convection on heat transfer and  
344 highlighted that natural convection was capable of dominating the heat transfer process, often minimizing the differences  
345 between various heat exchanger designs.

346 In the case of the discharge of latent heat results, there were obvious differences in comparing heat exchanger designs  
347 and thermal energy material composition. Toroid squiggle heat exchanger exhibited prolonged holding time of the heat  
348 energy output above 100 W and 50 W. Heat energy output above 100 W was retained for 0:09 – 0:11 [hh:mm] in the  
349 case of toroid squiggle heat exchanger and 0:05 – 0:08 [hh:mm] by spiral heat exchanger. Heat energy outputs exceeding  
350 50 W were maintained for 0:23 – 0:29 [hh:mm] in the case of spiral heat exchanger and 0:32 – 0:35 [hh:mm] in the case  
351 of toroid squiggle heat exchanger. The time ranges were higher in spiral heat exchangers, exhibiting higher sensitivity  
352 to the accumulation of substance composition for this particular heat exchanger design for this application. The findings  
353 were in accordance with the study of Oudaoui et al. [33], which highlighted the importance of heat exchanger design  
354 in improving thermal performance during the latent heat discharge of PCMs. The influence of various designs of heat  
355 transfer surfaces in PCM heat storage units was also discussed by Sultan et al. [34], demonstrating that the proper shape  
356 of these surfaces can enhance heat transfer from the phase change material to the surroundings.

357 In the case of the spiral heat exchanger, with the increase in SAT mass concentration in the accumulation substance, the  
 358 time also  
 359 be correlated with the maximal attained heat energy output value, which also upsurged with the increase of SAT mass  
 360 concentration in the accumulation substance. This was given by a lower amount of ballast in the form of added water,  
 361 which must be heated simultaneously with the latent heat of the SAT during the solidification process after the initiation  
 362 [28]. This phenomenon was also connected with the maximal reached temperature of the accumulation substance, which  
 363 was measured indirectly on the outer surface of the module (temperatures T3 and T4). In the case of the spiral heat  
 364 exchanger, which was characterised by lower heat energy output in the first stage of the discharging procedure after  
 365 initiation, the trend of heightening material temperature with increasing mass fraction of the SAT was obvious. The  
 366 same trend was not detected in the toroid squiggle heat exchanger due to higher heat energy output in the initial stage  
 367 of the discharging procedure after initiation, which does not allow warming up the outer surface of the module  
 368 accordingly. This outcome was in accordance with the abovementioned studies of Oudaoui et al. [33] and Sultan et al.  
 369 [34] that have described the importance of the heat exchanger shape during the phase changes.

370 The withholding time for heat energy output above 50 W was not significantly affected by the composition of the  
 371 accumulation substance in the toroid squiggle heat exchanger. In contrast, the spiral heat exchanger revealed a decrease  
 372 in holding time with an increase in the mass fraction of SAT in the accumulation substance. This must have been due  
 373 to poorer heat flux in the solid material and longer distances between the solidified accumulation substance and the heat  
 374 exchanger surface compared to the toroid squiggle heat exchanger [36]. The initial temperature of the accumulation  
 375 mixture during crystallisation, as described by Dannemand et al. [17], did not affect the results as it was always  
 376 equivalent to the laboratory temperature at initiation.

377 Approximately 50 minutes after initiation, the poorer heat flux from the accumulation substance to the heat exchanger,  
 378 and consequently to the heated medium, resulted in higher heat energy outputs for the spiral heat exchanger compared  
 379 to the toroid squiggle heat exchanger. This was mainly due to less heat being removed in the first stage of the latent heat  
 380 discharge phase. Additionally, the accumulation substance in the spiral heat exchanger displayed higher temperatures  
 381 after 50 minutes than in the toroid squiggle heat exchanger. Due to the wider heat output possibilities, the toroid squiggle  
 382 shape was observed to be a more suitable heat exchanger design.

383

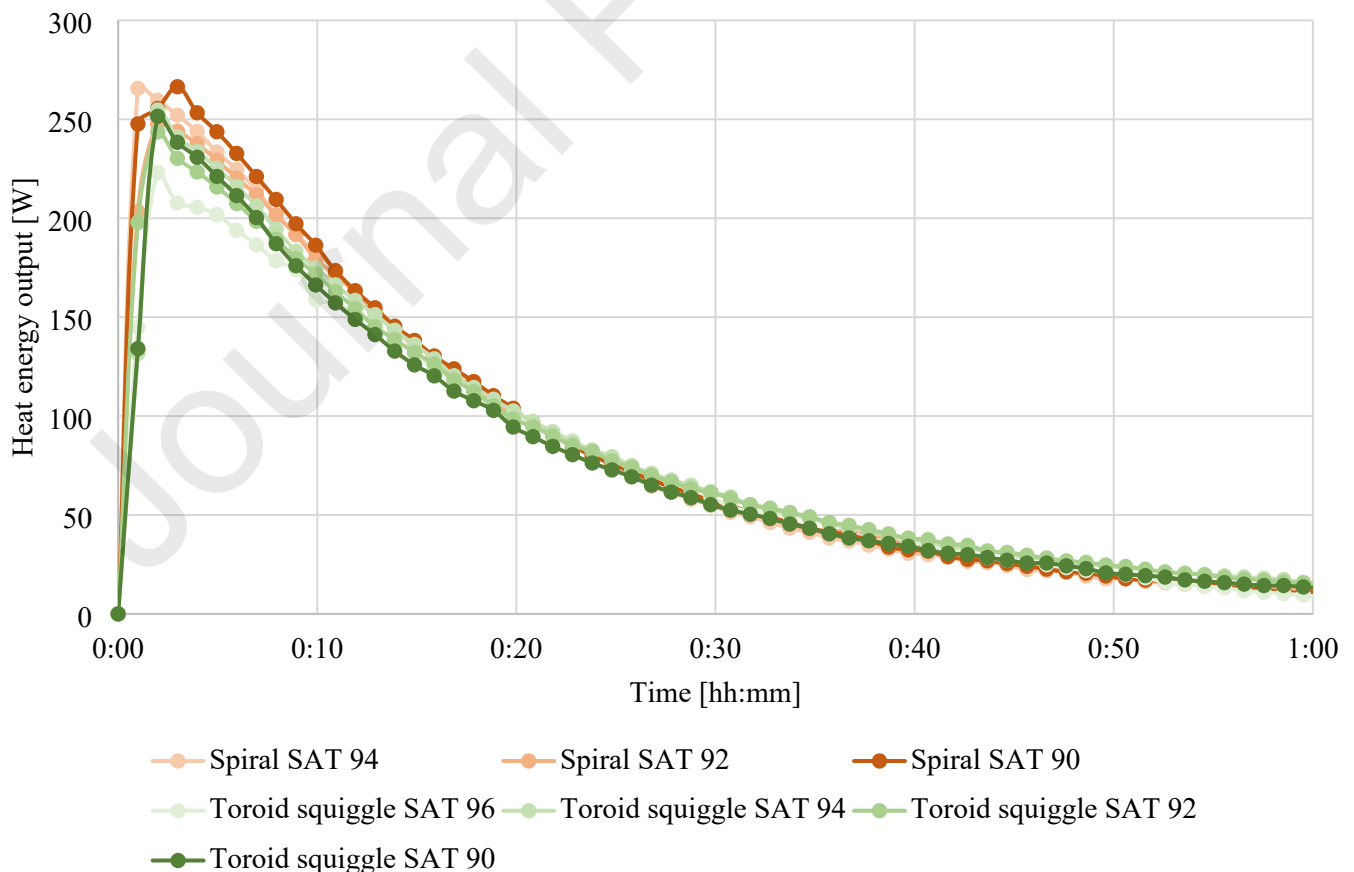
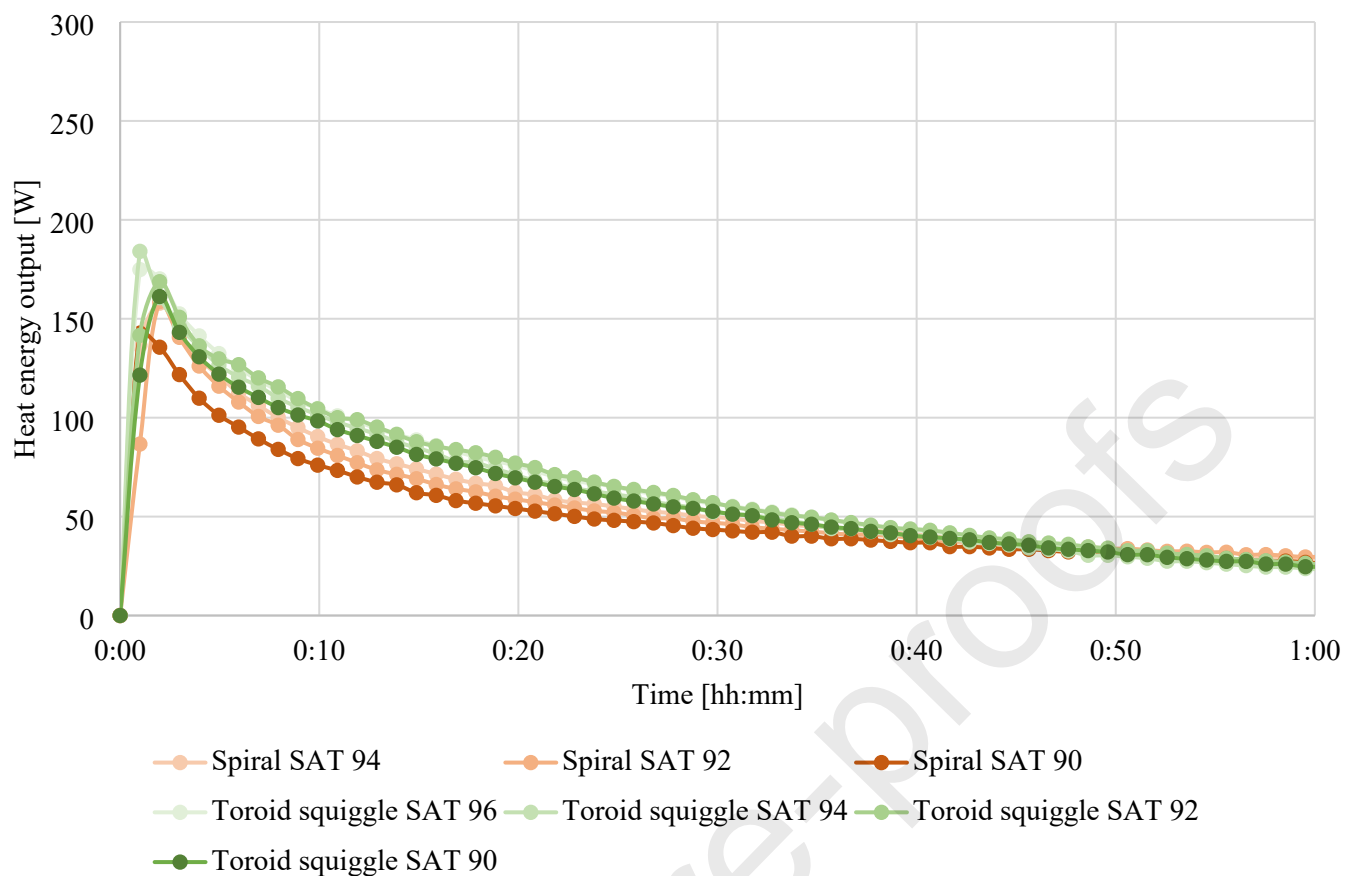


Fig. 4. Time courses of the heat energy output during the discharge of sensible heat phase



387

388

Fig. 5. Time courses of the heat energy output during the discharge of latent heat phase

389

Table 5 Holding times of heat energy output above 100 W and 50 W, respectively

Heat exchanger	Accumulation substance	$Q_{char\_teor}$	$Q_{sen\_teor}$	$Q_{L\_teor}$	$Q_{char\_real}$	$Q_{sen\_real}$	$Q_{L\_real}$	$Q_{char\_diff}$	$Q_{sen\_diff}$	$Q_{L\_diff}$
[-]	[%]	[Wh]	[Wh]	[Wh]	[Wh]	[Wh]	[Wh]	[%]	[%]	[%]
Spiral	SAT 94	180.7	92.2	100.6	$215.3 \pm 2.68$	$89.2 \pm 2.14$	$87.8 \pm 4.56$	19.2	3.2	12.7
Spiral	SAT 92	174.6	92.6	93.6	$207.8 \pm 3.05$	$89.6 \pm 2.61$	$88.0 \pm 7.25$	19.0	3.2	6.0
Spiral	SAT 90	172.2	96.2	86.7	$207.0 \pm 2.74$	$90.9 \pm 1.98$	$78.2 \pm 4.03$	20.2	5.5	9.8
Toroid squiggle	SAT 96	181.8	79.6	107.5	$227.0 \pm 3.16$	$83.1 \pm 1.70$	$85.0 \pm 4.44$	24.9	4.4	20.9
Toroid squiggle	SAT 94	184.5	94.4	100.6	$212.9 \pm 2.77$	$93.0 \pm 2.86$	$80.6 \pm 3.32$	15.4	1.5	19.9
Toroid squiggle	SAT 92	180.7	98.9	93.6	$214.6 \pm 3.26$	$88.2 \pm 3.12$	$81.9 \pm 3.57$	18.8	10.8	12.5
Toroid squiggle	SAT 90	173.3	97.3	86.7	$182.3 \pm 2.79$	$86.1 \pm 2.36$	$80.5 \pm 3.60$	5.2	11.5	7.1

391 All heat energy values were calculated according to the actual temperatures of the accumulation substance at the  
392 beginning and end of the phases, affecting the final values. The initial temperature of the module and the temperatures  
393 after the discharge phases ranged between 20 and 24 °C (laboratory temperature), the final temperature after the charging  
394 phase ranged between  $76 \pm 0.4$  and  $82 \pm 0.4$  °C and the temperature after the solidification ranged between  
395  $54.5 \pm 0.4$  and  $57 \pm 0.4$  °C.

396 Since the mass of the accumulation substance (1,750 g) was used as the reference value, the overall theoretical heat  
397 required to charge the system—i.e., to heat the entire module and liquefy the accumulation substance—decreased as the  
398 mass concentration of SAT was reduced. This reduction, though slightly influenced by the temperature range, had a  
399 significant impact on the actual latent heat energy required for complete liquefaction. The difference between SAT 90  
400 and SAT 96 was almost 20% of the latent heat energy.

401 All measured charge heat energy values were higher than the theoretical ones, ranging from 5.2% to 24.9% above  
402 expectations. Although the insulation shell was designed to fit the accumulation module perfectly, heat losses from the  
403 module were still prevalent. These losses were further exacerbated by the need to overheat the substance beyond the  
404 target temperatures described above.

405 SAT 96 was not tested with the spiral heat exchanger due to the instability of the accumulation mixture, as demonstrated  
406 in the experiments with the Torroid squiggle heat exchanger, which revealed partial crystallization throughout the entire  
407 module volume (Fig. 6 (A)). Moreover, SAT 96 exhibited the highest  $Q_{\text{char\_diff}}$  value, reducing the efficiency of heat  
408 storage. Given these findings, SAT 96 was deemed unsuitable for long-term heat energy storage and was therefore  
409 excluded from further testing with the spiral heat exchanger.

410 A study by Dannemand et al. [37] has shown that heat loss in accumulation modules using sodium acetate trihydrate  
411 can significantly impact the overall efficiency of the system. For instance, the heat loss characteristics of supercooled  
412 sodium acetate trihydrate were thoroughly investigated, revealing substantial differences between theoretical and real  
413 heat energy values due to heat loss and convection effects. The same study also highlighted the seasonal efficiencies,  
414 and the ratios of the latent heat energy stored to all energy needed for liquefaction, while the reached value was 39 %.

415 The differences between the theoretical and real heat energy released during the sensible heat discharge phase ranged  
416 between 1.5 and 11.5 %, influenced by the heat loss of the module and the measurement of the accuracy of the device  
417 (a significant part of the cooling process with a temperature difference of 0.2 °C). Another significant effect of the heat  
418 released during the sensible heat discharge phase is partial crystallization, which is accompanied by the release of latent  
419 heat. This process significantly reduced the  $Q_{\text{char\_diff}}$  value. Partial crystallization was observed in the cases of SAT 96  
420 and SAT 94. Figure 5 shows photographs of the accumulation modules containing the accumulation substances SAT  
421 96, SAT 94, and SAT 92.

422 Similar observations were made by Kong et al.[38], where partial crystallisation was reported for substances with water  
423 contents ranging from 40 % to 46 %. Their findings indicated that substances with 40 % and 42 % water content  
424 (corresponding to SAT 99 and SAT 96) exhibited partial crystallisation after long-term storage. In contrast, substances  
425 with 45% and 46% water content (corresponding to SAT 93 and SAT 91) remained free of partial crystallisation. These  
426 results are consistent with the findings presented in this current study.



Fig. 6. Accumulation substance state after liquefaction and cool down to laboratory temperature; from left: SAT 96, SAT 94, SAT 92

Despite the partial crystallization occurrence, it was never observed that initiation was spontaneously triggered (after all liquefaction processes, there was latent heat energy stored). Instead, initiation was consistently triggered in a controlled manner, as required during the presented experiments. This behaviour was in contrast with the experimental 150 L storage modules described in the study by Dannemand et al. [23], where uncontrolled initiated crystallization occurred in most instances. One more study by Dannemand et al. [37] also described the uncontrolled initiation triggering in 13 of 20 experiments.

The larger volume of the modules in these studies (150 L) compared to the smaller volume of approximately 2 L in the presented study could be a significant factor. Larger volumes were more prone to temperature gradients and uneven (local) cooling, which resulted in spontaneous crystallization. As spontaneous crystallisation is also a statistical process, it is also more likely that a growing crystal will cross the crystallisation barrier in a larger volume.

Furthermore, the glass and copper used in our modules, provided better thermal conductivity and more uniform temperature distribution, reducing the likelihood of partial crystallization [39]. High-volume, custom-made accumulation modules can also suffer from impurities, which could affect the behaviour of the accumulation substance.

From the latent heat point of view, the difference between theoretical and real values ranged between 6 and 20.9 %, while the highest differences were obtained for the higher mass fraction of SAT in the accumulation substance, which was associated with the partial crystallisation of the accumulation substance and consequent emission of part of the latent heat during the sensible heat discharge phase.

Specific heat capacity provided an indication of the amount of energy required to heat one unit of mass of the substance that resulted in an increase of one unit in temperature. Specific heat capacities were measured for SAT 92 and SAT 90 to scrutinize the differences between these two partials crystallisation-free samples and to determine the values of phase change of SAT/water mixtures. The values of onset and peak temperatures and related specific heat capacities were evaluated from Fig. 7 and have been summarized in Table 6.

- $T_0$  (onset temperature) marks the initiation of thermal activity in the solid phase. For SAT 92 and SAT 90, these  $T_0$  were set at 14.9 °C and 14.7 °C, respectively, indicating the beginning of the measurement and, therefore, the beginning of measured specific heat capacity changes.

457  
458

- $T_i$  (onset of the liquid phase) signals the transition from solid to liquid state, which is critical for phase-change

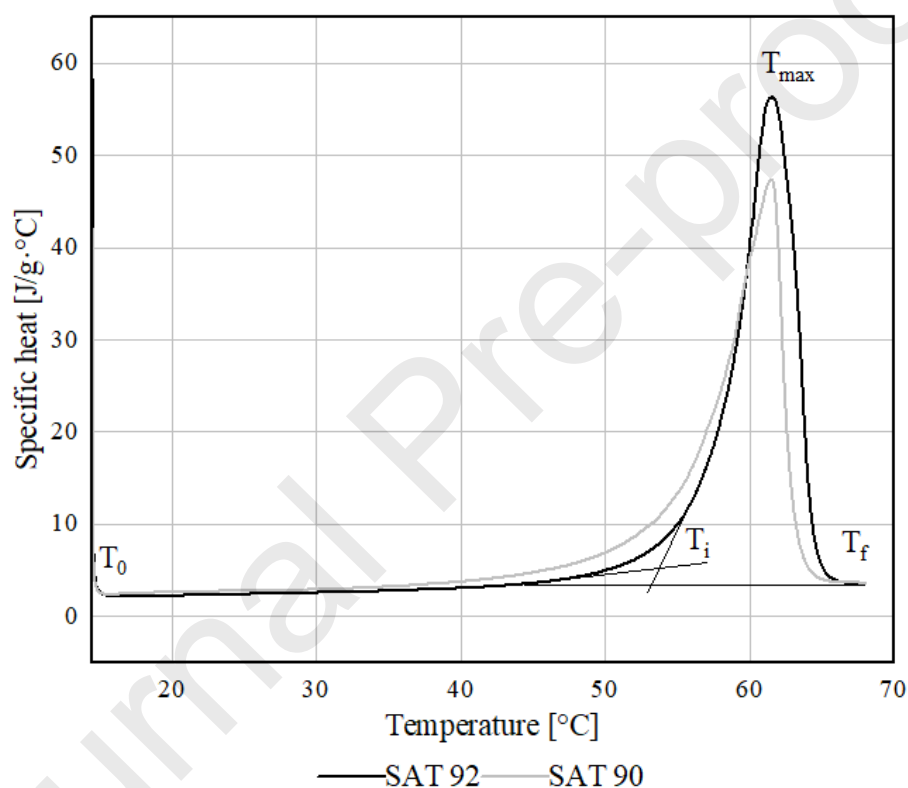
459  
460  
461  
462

- $T_{max}$  (peak temperature) reflects the temperature at which the phase change is most active, releasing or absorbing significant energy. SAT 92 and SAT 90 exhibit similar peak temperatures of 61.6 °C and 61.5 °C, respectively.
- $T_f$  (final temperature) indicates the completion of phase transition, stabilizing the liquid state (end of the measurement).

463  
464  
465  
466  
467

The phase change temperature of SAT 92 and SAT 90 were less than the melting temperature of pure SAT (58 °C), as reported in the literature ([40]). The specific heat showcased a smoother rising trend in the pure solid phase, followed by a sharp upsurge between the solid-liquid transitions as the temperature heightened. The increase of specific heat capacities for the samples SAT 92 and SAT 90 was apparent in comparison with pure SAT (the values of 2.1 kJ/kg·K in the solid state and 3.0 kJ/kg·K in the liquid state [40]).

468  
469



470  
471

Fig. 7. Specific heat capacities (J/g·°C) of the samples SAT92 and SAT90.

472  
473  
474  
475  
476  
477  
478  
479  
480

The comparison in Fig. 7 highlighted smoother specific heat capacity curves in the solid state, followed by sharp increases during phase transitions. The higher specific heat capacities of SAT 90 (2.4 J/g·°C in the solid phase and 5.1 J/g·°C in the liquid phase) compared to SAT 92 described its energy storage potential, possibly due to its higher water content. In this measurement methodology, the liquefaction process occurred over a broader temperature range rather than at a single specific temperature. In the case of SAT 90, an earlier increase in specific heat was evident from about 30 °C, whereas in the case of SAT 92 it was only evident from about 42 °C. The earlier rise in specific heat could be linked to differences in the thermal conductivity of the studied materials. Additionally, this value can be enhanced by additives such as  $Al_2O_3$  [41], copper Nano-particles [42] or copper formed into a foam[43], however these materials utilisation was observed to be beyond the scope of this study.

481

Specific heat capacity							
	Solid phase (T <sub>0</sub> )	Liquid phase (T <sub>i</sub> )	Liquid phase (T <sub>f</sub> )	Onset temperature (T <sub>0</sub> )	Onset temperature (T <sub>i</sub> )	Peak temperature (T <sub>max</sub> )	Final temperature (T <sub>f</sub> )
	[J/g·°C]	[J/g·°C]	[J/g·°C]	[°C]	[°C]	[°C]	[°C]
SAT 92	2.1	5.0	3.6	14.9	54.1	61.6	67.5
SAT 90	2.4	5.1	3.7	14.7	51.5	61.5	67.3

483

484 **CONCLUSIONS**

485 This study has effectively investigated the charge and discharge characteristics of a heat exchanger system during  
 486 sensible and latent heat storage phases, focusing on the impacts of heat exchanger designs and accumulation substance  
 487 compositions. The charge period consistently ranged from 2:50 to 3:27 [hh:mm], with varying discharge durations for  
 488 sensible and latent heat.

489 During the sensible heat discharge phase, both spiral and toroid squiggle heat exchanger designs exhibited comparable  
 490 performance, as free convection played a dominant role, equalizing differences between the designs. However, in the  
 491 latent heat discharge phase, significant differences emerged. The toroid squiggle exchanger sustained energy output  
 492 above 100 W for 11 minutes and above 50 W for 35 minutes, whereas the spiral exchanger retained above 100 W for  
 493 only 7 minutes and above 50 W for 26 minutes for SAT 92 mixture. These results highlight the superior thermal  
 494 performance of the toroid squiggle exchanger, making it a more efficient choice for practical energy storage applications.

495 A comparison between theoretical and real heat energy outputs revealed discrepancies due to factors such as heat loss,  
 496 free convection effects in liquid areas, and partial crystallization. For example, the real charge heat energy was 5.2% to  
 497 24.9% higher than the theoretical values, primarily due to heat losses and convection-driven energy redistribution within  
 498 the system. Additionally, the difference between theoretical and real latent heat discharge values ranged from 6% to  
 499 20.9%, with the highest differences observed in samples containing a higher mass fraction of sodium acetate trihydrate,  
 500 which experienced partial crystallization.

501

502 **Key Findings:**

- 503 • The sodium acetate trihydrate-to-water ratio of 92% (SAT 92) provided an optimal balance between phase  
 504 stability, low theoretical to real latent heat capacity and high energy retention, exhibiting a theoretical latent  
 505 heat capacity of 93.6 Wh.
- 506 • The toroid squiggle exchanger had maintained an energy output surpassing 100 W for 11 minutes and greater  
 507 than 50 W for 35 minutes, compared to 7 minutes and 26 minutes, respectively, for the spiral exchanger.
- 508 • Specific heat capacity measurements showed that SAT 92 exhibited values of 2.1 kJ/kg·K in the solid phase  
 509 and 5.0 kJ/kg·K in the liquid phase, confirming its strong potential for thermal energy storage applications.

510

511 The research findings of this study have underscored the importance of considering both heat exchanger design and  
 512 accumulation substance composition in optimising the performance of phase-change heat storage systems.

513 While this study provides valuable insights into optimizing metastable supercooled liquid phase change materials for  
 514 long-term heat storage, several challenges still remain unexplored. One key limitation is the experimental scale, which  
 515 focuses on small-scale modules, future research should explore larger-scale implementations to evaluate real-world

516 performance and scalability. Additionally, while the effect of sodium acetate trihydrate-to-water ratios on phase stability  
517 and Journal Pre-proofs ized  
518 formulations under varying environmental conditions. Another challenge is the relatively low thermal conductivity of  
519 sodium acetate trihydrate, which could be addressed by incorporating thermally conductive additives or composite  
520 materials. Future work should also focus on improving heat exchanger designs and exploring alternative PCM  
521 formulations to enhance efficiency and reliability. Conclusively, integration with renewable energy systems, such as  
522 solar thermal collectors or heat pumps, should be further explored to maximize the practical application of this  
523 technology.

## 525 ACKNOWLEDGEMENT

526 The preparation of this article was financed by The Technology Agency of the Czech Republic within the Delta 2  
527 Programme, project no.: "TM0400021". The European Union also financially supported this work under the  
528 REFRESH—Research Excellence For Region Sustainability and High-tech Industries project  
529 No.CZ.10.03.01/00/22\_003/0000048 via the Operational Programme Just Transition.

## 531 CREDIT AUTHOR STATEMENT

532 Jiří Ryšavý: Conceptualization, Methodology, Writing - Original draft preparation, Writing – review & editing, Project  
533 administration; Jakub Čespiva: Conceptualization, Methodology, Writing - Original draft preparation, Writing – review  
534 & editing, Project administration; Thangavel Sangeetha: review & editing; Cristian Teicht: Writing – review & editing;

535 Matěj Charvát: Data curation; Wei-Mon Yan: Validation, Supervision; Ricardo Chacartegui: review & editing; Tadeáš  
536 Ochodek: Supervision;

- 537
- 538 [1] Wu S, Hall MR. 4 - Heat energy storage and cooling in buildings. *Materials for Energy Efficiency and Thermal*  
539 *Comfort in Buildings*. Woodhead Publishing; 2010, p. 101-26.
- 540 [2] Radner F, Strobl N, Köberl M, Rauh J, Esser K, Winkler F, et al. How to size regional electrolysis systems -  
541 Simple guidelines for deploying grid-supporting electrolysis in regions with renewable energy generation.  
542 *Energy Conversion and Management: X* 2023;20 C7 - 100502.
- 543 [3] Chu W, Duić N, Wang Q. Recent advances in energy storage and energy saving technologies: SDEWES special  
544 issue in 2022. *Energy Storage and Saving* 2024;3(1):1-4.
- 545 [4] Hackenberg A, Kappertz L, Rapol S, Solovievskyi V, Büskens C. Optimal dimensioning of renewable energy  
546 generation and storage systems. *Energy Conversion and Management: X* 2024;24 C7 - 100773.
- 547 [5] Venkateswarlu K, Ramakrishna K. Recent advances in phase change materials for thermal energy storage-a  
548 review. *JOURNAL OF THE BRAZILIAN SOCIETY OF MECHANICAL SCIENCES AND ENGINEERING*  
549 2022;44(1).
- 550 [6] Afaynou I, Faraji H, Choukairy K, Khallaki K, Akrou D. Effectiveness of a PCM-based heat sink with partially  
551 filled metal foam for thermal management of electronics. *INTERNATIONAL JOURNAL OF HEAT AND*  
552 *MASS TRANSFER* 2024;235.
- 553 [7] Cuce E, Cuce P, Saxena A, Guclu T, Besir A. Performance analysis of a novel solar desalination system - Part  
554 1: The unit with sensible energy storage and booster reflector without thermal insulation and cooling system.  
555 *SUSTAINABLE ENERGY TECHNOLOGIES AND ASSESSMENTS* 2020;37.
- 556 [8] Cuce P, Cuce E, Tonyali A. Performance analysis of a novel solar desalination system - Part 2: The unit with  
557 sensible energy storage with thermal insulation and cooling system. *SUSTAINABLE ENERGY*  
558 *TECHNOLOGIES AND ASSESSMENTS* 2021;48.

- 559 [9] Assareh E, Keykhah A, Hoseinzadeh S, Astiaso Garcia D. Application of PCM in a Zero-Energy Building and  
560 Journal Pre-proofs 17).
- 561 [10] Ceylan I, Gürel A, Ergün A, Ali I, Agbulut Ü, Yildiz G. A detailed analysis of CPV/T solar air heater system  
562 with thermal energy storage: A novel winter season application. JOURNAL OF BUILDING ENGINEERING  
563 2021;42.
- 564 [11] Cuce PM, Kolayli S, Cuce E. Enhanced performance figures of solar cookers through latent heat storage and  
565 low-cost booster reflectors. International Journal of Low-Carbon Technologies 2020;15(3):427-33.
- 566 [12] Saxena A, Cuce E, Singh D, Sethi M, Cuce P, Sagade A, et al. Experimental studies of latent heat storage based  
567 solar air heater for space heating: A comparative analysis. JOURNAL OF BUILDING ENGINEERING  
568 2023;69.
- 569 [13] Arumugam C, Shaik S, Roy A, Kontoleon K, Cuce E, Shaik A, et al. Analysis of the benefits of adopting roof  
570 sandwich panels integrated with PCM versus PUR to mitigate energy costs and carbon dioxide emissions.  
571 JOURNAL OF ENERGY STORAGE 2024;77.
- 572 [14] Morciano M, Fasano M, Chiavazzo E, Mongibello L. Trending applications of Phase Change Materials in  
573 sustainable thermal engineering: An up-to-date review. ENERGY CONVERSION AND MANAGEMENT-X  
574 2025;25.
- 575 [15] Safari A, Saidur R, Sulaiman F, Xu Y, Dong J. A review on supercooling of Phase Change Materials in thermal  
576 energy storage systems. RENEWABLE & SUSTAINABLE ENERGY REVIEWS 2017;70:905-19.
- 577 [16] Wang G, Xu C, Kong W, Englmaier G, Fan J, Wei G, et al. Review on sodium acetate trihydrate in flexible  
578 thermal energy storages: Properties, challenges and applications. JOURNAL OF ENERGY STORAGE  
579 2021;40.
- 580 [17] Dannemand M, Delgado M, Lazaro A, Penalosa C, Gundlach C, Trinderup C, et al. Porosity and density  
581 measurements of sodium acetate trihydrate for thermal energy storage. Applied Thermal Engineering  
582 2018;131:707-14.
- 583 [18] Zalba B, Marín JM, Cabeza LF, Mehling H. Review on thermal energy storage with phase change: materials,  
584 heat transfer analysis and applications. Applied Thermal Engineering 2003;23(3):251-83.
- 585 [19] Zhao BC, Li TX, Gao JC, Wang RZ. Latent heat thermal storage using salt hydrates for distributed building  
586 heating: A multi-level scale-up research. Renewable and Sustainable Energy Reviews 2020;121:109712.
- 587 [20] Beaupere N, Soupremanien U, Zalewski L. Influence of water addition on the latent heat degradation of sodium  
588 acetate trihydrate. Applied Sciences (Switzerland) 2021;11(2 C7 - 484):1-17.
- 589 [21] Wang S, Wang C, Hussain MB, Cheng X, Wang Z. Study on performance improvement of sodium acetate  
590 trihydrate in thermal energy storage system by disturbance. Processes 2022;10(6):1093.
- 591 [22] Dannemand M, Dragsted J, Fan J, Johansen JB, Kong W, Furbo S. Experimental investigations on prototype  
592 heat storage units utilizing stable supercooling of sodium acetate trihydrate mixtures. Applied Energy  
593 2016;169:72-80.
- 594 [23] Dannemand M, Johansen JB, Kong W, Furbo S. Experimental investigations on cylindrical latent heat storage  
595 units with sodium acetate trihydrate composites utilizing supercooling. Applied Energy 2016;177:591-601.
- 596 [24] Englmaier G, Furbo S, Dannemand M, Fan J. Experimental investigation of a tank-in-tank heat storage unit  
597 utilizing stable supercooling of sodium acetate trihydrate. Applied Thermal Engineering 2020;167:114709.
- 598 [25] Kafle BP, Devkota S, Uprety B, Park KY, Basnet N, Shakya A, et al. Storing Solar Energy in Sodium Acetate-  
599 Based Hand Warmers Using Light-Absorbing Particles. ACS Applied Energy Materials 2020;3(12):11772-80.
- 600 [26] Nohejl E. Seasonal heat accumulator with minimal losses. TzB-info 2014;6.

- 601 [27] Dannemand M, Johansen JB, Furbo S. Solidification behavior and thermal conductivity of bulk sodium acetate  
602 Journal Pre-proofs  
603 2016;145:287-95.
- 604 [28] Beaupere N, Soupremanien U, Zalewski L. Experimental measurements of the residual solidification duration  
605 of a supercooled sodium acetate trihydrate. INTERNATIONAL JOURNAL OF THERMAL SCIENCES  
606 2020;158.
- 607 [29] Babaharra O, Choukairy K, Faraji H, Khallaki K, Hamdaoui S, Bahammou Y. Thermal performance analysis  
608 of hollow bricks integrated phase change materials for various climate zones. Heat Transfer 2024;53(4):2148-  
609 72.
- 610 [30] Yazdani M, Laitinen A, Helaakoski V, Farnas L, Kukko K, Saari K, et al. Efficient storage and recovery of  
611 waste heat by phase change material embedded within additively manufactured grid heat exchangers.  
612 INTERNATIONAL JOURNAL OF HEAT AND MASS TRANSFER 2021;181.
- 613 [31] Tian Y, Zheng M, Fan D, Zhang Y, Zhao J, Jin G, et al. A novel latent heat storage unit by introducing jet  
614 breakup of phase change material. JOURNAL OF ENERGY STORAGE 2022;49.
- 615 [32] Fichema. Product datasheet Sodium acetate trihydrate (2023). Brno, Czech Republic: Fichema; 2023.
- 616 [33] Oudaoui K, Faraji M. Numerical Study of Latent Heat Discharge of a Phase Change Material Shell-and-Tube  
617 Thermal Energy Storage System. Cham: Springer Nature Switzerland; 2024:151-9.
- 618 [34] Sultan HS, Mohammed HI, Biswas N, Togun H, Ibrahim RK, Mahdi JM, et al. Revolutionizing the latent heat  
619 storage: Boosting discharge performance with innovative undulated phase change material containers in a  
620 vertical shell-and-tube system. Journal of Computational Design and Engineering 2024;11(2):122-45.
- 621 [35] Garoosi F, Hoseininejad F, Rashidi M. Numerical study of natural convection heat transfer in a heat exchanger  
622 filled with nanofluids. ENERGY 2016;109:664-78.
- 623 [36] Kothandaraman CP. Fundamentals of Heat and Mass Transfer. New Age International (P) Ltd.; 2006.
- 624 [37] Dannemand M, Kong W, Fan J, Johansen JB, Furbo S. Laboratory Test of a Prototype Heat Storage Module  
625 Based on Stable Supercooling of Sodium Acetate Trihydrate. Energy Procedia 2015;70:172-81.
- 626 [38] Kong W, Dannemand M, Johansen JB, Fan J, Dragsted J, Englmaier G, et al. Experimental investigations on  
627 heat content of supercooled sodium acetate trihydrate by a simple heat loss method. Solar Energy 2016;139:249-  
628 57.
- 629 [39] Oliver DE, Bissell AJ, Liu X, Tang CC, Pulham CR. Crystallisation studies of sodium acetate trihydrate-  
630 suppression of incongruent melting and sub-cooling to produce a reliable, high-performance phase-change  
631 material. CrystEngComm 2021;23(3):700-6.
- 632 [40] Dannemand M, Schultz J, Johansen J, Furbo S. Long term thermal energy storage with stable supercooled  
633 sodium acetate trihydrate. APPLIED THERMAL ENGINEERING 2015;91:671-8.
- 634 [41] Roy A, Venkataraj KP, Vigneshwaran P, Saboor S, Cuce E, Saxena KK. Enhanced convective heat transfer with  
635 Al<sub>2</sub>O<sub>3</sub>-water nanofluid in a PCM-based thermal energy storage system. Journal of Energy Storage 2024;97 C7  
636 - 112853.
- 637 [42] Cui W, Yuan Y, Sun L, Cao X, Yang X. Experimental studies on the supercooling and melting/freezing  
638 characteristics of nano-copper/sodium acetate trihydrate composite phase change materials. RENEWABLE  
639 ENERGY 2016;99:1029-37.
- 640 [43] Zhao L, Xing Y, Liu X, Luo Y. Thermal performance of sodium acetate trihydrate based composite phase  
641 change material for thermal energy storage. APPLIED THERMAL ENGINEERING 2018;143:172-81.
- 642